



# Synthesis and characterization of n-type lightly doped mesoporous silicon nanowires through 1-MACE, influence of etching solution temperature

Somaye Ashrafabadi<sup>1</sup> · Hosein Eshghi<sup>1</sup>

Received: 4 September 2017 / Accepted: 16 January 2018 / Published online: 30 January 2018  
© Springer Science+Business Media, LLC, part of Springer Nature 2018

## Abstract

In this paper, large-area arrays of vertical and orderly mesoporous silicon nanowires (SiNWs) were fabricated through one-step metal assisted chemical etching (1-MACE) process using lightly doped n-Si substrate. Etching occurred in HF/ AgNO<sub>3</sub>/ H<sub>2</sub>O<sub>2</sub> solution. Field emission scanning electron microscopy (FESEM), and transmission electron microscopy (TEM) revealed that the whole surfaces of nanowires (NWs) are covered by dense mesoporous structures. Furthermore, the effect of solution etching temperature on morphological, optical and vibrational properties of SiNWs was investigated. FESEM images showed that the lengths of NWs are increased by increasing etching temperature, but the diameter changes are slight. Selected area electron diffraction (SAED) patterns indicate that the SiNWs formed at room temperature (RT) have single crystal structure, while those prepared at higher temperatures have polycrystal structure. In addition, the average reflectance is significantly low, i.e. less than 0.1% for SiNWs, in the wavelength range of 400–1100 nm. Also, a visible photoluminescence (PL) was observed in the samples, which is attributed to the silicon nano crystallites (SiNCs) decorated on the wall of NWs. The size of SiNCs is calculated through a frequency shift in the Raman spectrum. The optically active mesoporous SiNWs open new opportunities for nanoscale optoelectronic devices.

## 1 Introduction

Nanoscale silicon has garnered substantial attention due to its potential to impacts on broad areas ranging from nano-electronics, photonics, optoelectronics, photocatalysts, photovoltaics, [1, 2], Li-ion batteries [3] renewable energy to biochemical sensors [4]. Recently, Silicon nanowires in particular have drawn wide interest of researchers, owing to their special one-dimensional physical morphology and biocompatibility [5, 6]. Silicon Nano Wires (SiNWs) and porous silicon have prominent properties of antireflection and photoluminescence, respectively [3], which lead to particular concern and study. A combination of these two advantages and the formation of a novel composite nano-structure, porous silicon nanowires (pSiNWs) was suggested. This new structure has been applied in a new generation of silicon based optoelectronics over the past decade

[3, 6, 7]. Various approaches which require expensive equipment and involving complicated operation such as high temperature processing, and high-vacuum environment, have been developed to synthesize SiNWs, [1, 8]. To overcome these disadvantages, a simple and low cost method, metal-assisted chemical etching (MACE), has been developed recently [9–11]. This synthetic technique provides better structure controllability of SiNW such as diameter, length, orientation, morphology and porosity. Usually pSiNWs are fabricated through MACE method. Primarily, the MACE contains two steps: 1—the deposition of metal nanoparticles, which acts as a catalyst, and 2—the etching of the silicon in an etchant solution contains HF [3]. According to that, these two procedures occur separately or simultaneously, it is classified as two-step (2-MACE) and one-step MACE (1-MACE) respectively. In the 1-MACE simplified method, the nucleation of metal nanoparticles and the etching occur in an aqueous solution containing HF, metal salt (AgNO<sub>3</sub>) and H<sub>2</sub>O<sub>2</sub> as the oxidizing agent [12]. The mesoporous (pore size: 2–50 nm) silicon nanowires (mp-SiNWs) have a great potential of wide applications derived from the enhanced surface areas to volume ratio and quantum confinement effect. The doped type and level, fabrication methods and

✉ Hosein Eshghi  
h\_eshghi@shahroodut.ac.ir

<sup>1</sup> Faculty of Physics, Shahrood University of Technology, Shahrood, Iran

etching temperature have an important effect on the morphology of SiNWs. In general, for both 1-MACE and 2-MACE, it is not easy to obtain pSiNWs from medially or lightly doped silicon wafers [5, 13]. It has been reported that both p- and n-type mp-SiNWs can be obtained through 2-MACE [6, 14, 15], and using 1-MACE can result to p-type mp-SiNWs but rough n-type SiNWs without pores regardless of the doped level [5]. To et al. [5] reported that the mp-SiNWs were also obtained from heavily doped (1–5 mΩ cm) n-type silicon by the 1-MACE method. Chen et al. [16] have reported the fabrication of porous silicon nanowires using n-Si (1–10 Ω cm), through 1-MACE at 60 and 80 °C.

In this work, mp-SiNWs were obtained using lightly doped n-type silicon wafer through 1-MACE process, at room temperature (RT). Furthermore, the effect of etching solution temperature on the physical properties of mp-SiNWs was studied.

## 2 Materials and methods

The lightly doped n-type Si (100) wafer with resistivity of 0.22 Ω cm was used as the starting substrate material. Prior to etching, the wafer was cut into 1 × 1 cm<sup>2</sup> and then cleaned using acetone and ethanol in the ultrasonic condition at room temperature (RT) for 10 and 5 min, respectively, in order to remove the probable organic grease on the surface. The samples were then put in the hot Piranha solution (98% H<sub>2</sub>SO<sub>4</sub>/30% H<sub>2</sub>O<sub>2</sub> = 3:1 v/v) for 20 min. Then the substrates were immersed into DI-H<sub>2</sub>O: HF 40% (10:1; v/v) for 3 min to remove the native oxide. Afterwards, the Si samples were immediately placed into the 4.6 M HF/ 0.02 M AgNO<sub>3</sub>/ 0.1 M H<sub>2</sub>O<sub>2</sub> etching solution at different temperatures (RT, 50 and 75 °C) for 80 min in a plastic beaker. These samples are called N25, N50 and N75, respectively. Finally, the samples were immediately dipped into HNO<sub>3</sub> to dissolve the as-generated Ag dendrites. After each acid treatment the substrates were thoroughly rinsed in deionized water. The fabrication conditions of the studied samples are listed in Table 1.

The morphology of SiNWs covered on the surface was characterized by field emission scanning electron microscopy (FESEM) (Hitachi S. 4160) and transmission electron microscopy (TEM) (CM 30, 300 kV). The crystallinity of samples was studied by selected area electron diffraction (SAED) patterns (SAED, integrated with CM30 300 kV TEM). For the TEM and SAED analyses, SiNWs were scratched off from the n-Si substrates and collected on a copper grid. Then, several drops of ethanol was spread on the copper grid. Afterwards, the grid was dried at room temperature and inspected by TEM. Also the reflectance spectra (Shimadzu UV–Vis.1800) of SiNWs in the visible region were investigated. The Raman spectra was obtained by a

**Table 1** The details of fabrication conditions of the synthesized samples

Sample code	AgNO <sub>3</sub> concentration (mol/L)	HF concentration (mol/L)	H <sub>2</sub> O <sub>2</sub> concentration (mol/L)	Etching time (min)	Etching temperature (°C)
N25	0.02	4.6	0.1	80	25
N50	0.02	4.6	0.1	80	50
N75	0.02	4.6	0.1	80	75

Takram P50C0R10 system equipped with a 532 nm source. Moreover, we have used an analytical model for determination of the silicon crystallite size through Raman spectra of the samples [1, 11]. The photoluminescence (PL) spectra were measured using a 320 nm laser as the exciting photon wavelength.

## 3 Results and discussion

### 3.1 Surface morphological analysis

Figure 1 shows the top and side views of FESEM images for N25 sample. As it is clear it is covered with orderly and dense SiNW arrays. The vertical orientation of these arrays are attributed to the fact that the direction <100> has the smallest energy barrier for etching [17]. As it is evident, the SiNWs get together on top and have a bundle-like structure, as a result of increment of strain in the presence of numerous porous structures and Van der Waals force between the nanowires [3, 13]. According to Fig. 1b the length of SiNWs is 10 μm and their diameter is in the range of 100–200 nm. For further study on the nanostructure and crystallinity of SiNWs, TEM characterizations were used (Fig. 1c). As the TEM image of a typical nanowire shows, the surface is covered with dense and homogeneous mesoporous structure. The SAED pattern (the inset in Fig. 1c) shows a single crystal-like diffraction pattern, which indicates that mp-SiNWs in N25 has preserved the single crystalline structure of its starting Si wafer. The single crystalline nature of mp-SiNWs implies the etching process does not damage the integrity and continuity of the silicon lattice [3].

In order to describe the formation of mp-SiNWs, it is necessary to review the etching mechanism. The AgNO<sub>3</sub> role in the etching process is to work as the oxidant and provide silver particles to act as catalysts [6]. When lightly doped silicon wafer is dipped into the etchant, its surface is covered with the Ag dendritic layer. As the standard reduction potential of H<sub>2</sub>O<sub>2</sub> (1.77 eV) is larger than that of Ag (0.78 eV), the as-generated Ag dendrites are oxidized into Ag<sup>+</sup> ions by H<sub>2</sub>O<sub>2</sub> (Eq. 1). Electrons preferentially transport from silicon to Ag<sup>+</sup> ions due to the more negative valence band of silicon

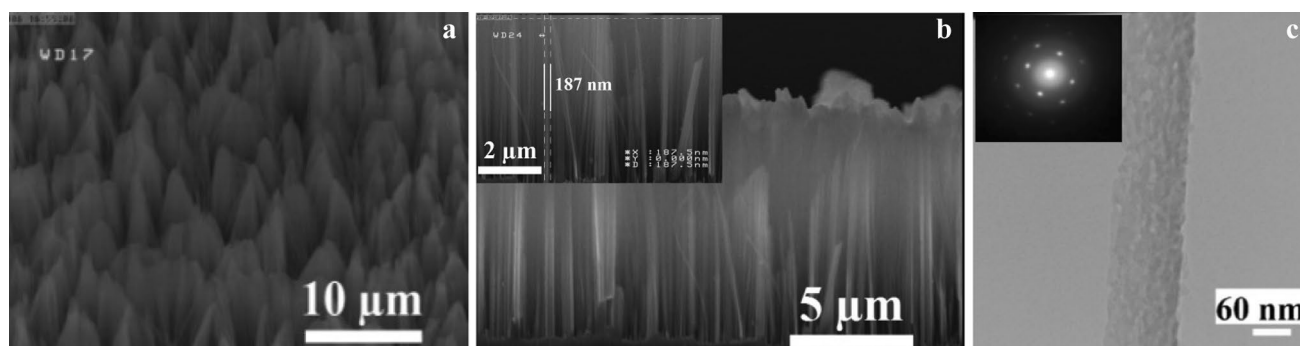
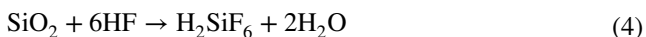
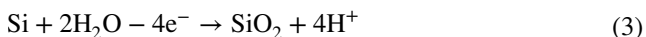
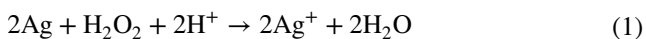


**Fig. 1** **a** Oblique (scale 10  $\mu\text{m}$ ) and **b** cross-section FESEM images of N25 (scales 5 and 2  $\mu\text{m}$ , the inset). **c** TEM image and SAED pattern (the inset) of one of typical wires of this sample

compared with the redox potential of Ag (or holes inject to the conduction band of silicon) [5]. This electron transportation results in nucleation of Ag nanoparticles (AgNPs) on the surface and oxidation of silicon (Eqs. 2 and 3). The oxidized  $\text{SiO}_2$  is dissolved by HF, so nanopits are formed underneath to capture the AgNPs and lead to the vertical etching of the substrate. The residual of the bulk silicon turns to vertical SiNW arrays which keep the properties of the starting wafer. The nucleation usually occurs at surface states, such as dangling bonds, crystal defects and sites around the impurities such as dopants [5]. SiNWs are decorated with self-grown SiNCs, which essentially form due to the sidewall etching and lead to porous structure nanowires [18]. While the etching time increases, all the large numbers of generated  $\text{Ag}^+$  ions are not re-nucleate during vertical etching. Therefore, extra  $\text{Ag}^+$  ions spread through the nanowires and trap electrons from the sidewalls. This behavior results in lateral etching of SiNWs and subsequently formation of mp-SiNWs decorated with SiNCs [3, 13, 18].



We proceeded our investigations with the same conditions for other two samples etched at 50 and 75, i.e. N50 and N75, respectively. Considering the oblique and cross section views of FESEM images in these samples (Figs. 2, 3, respectively), not only the morphology of them are obviously different from the one prepared at RT (sample N25), but also the lengths of SiNWs are increased to 25 and 60  $\mu\text{m}$  in N50 and N75, respectively, however, the diameter variations are slight. The Ag-nucleation usually occurs at the surface states, mainly around the impurities [5], and the SiNWs diameters are closely related to the

space between the metal particles, and the immersion time in the HF solution [19]. Accordingly, due to the fact that doping level and the etching time are the same in these samples, the diameter of the NWs changes slightly. For the length variation of NWs, it should be noted that the process II and IV are thermally excited via raising the etching temperature [9] and also at temperatures higher than RT, the  $\text{SiF}_6^{2-}$  ion will decompose to the volatile  $\text{SiF}_4$  gas, which result in faster etching [20]. Therefore, the vertical etching rate will increase and tend to longer NWs. From the TEM images (Fig. 4) of one of the typical nanowires in these samples, it is clear that numerous pores have covered the whole surface of these NWs, leading to the formation of mesoporous structures. Also, as it is obvious from SAED patterns (the inset in Fig. 4), high temperature etching layers (N50 and N75) showed poly-crystalline structures (ring patterns) whereas the room temperature sample (N25) showed single crystalline structure. The increment of temperature could result in higher porosity of NWs and subsequently the formation of NCs on the surface of NWs.

### 3.2 Optical properties

Figure 5 shows the reflectance spectra in our prepared SiNWs over the wavelength range of 400–1100 nm. According to these data, the average reflectance in the visible range (400–700 nm) is  $\sim 0.07\%$  and reaches to  $\sim 0.1\%$  in the infrared region (700–1100 nm). This drastic low reflectance could be attributed to the increase of photons scatterings in the created pores as a result of NWs formation on the surface of Si wafer, as all the samples seems black by the naked eye. Such a substantially low reflectance and subsequently expecting high absorbance in visible up to near infrared range, which is not achievable with the conventional anti-reflecting coatings, is suitable for the Si-based solar cell applications [21].

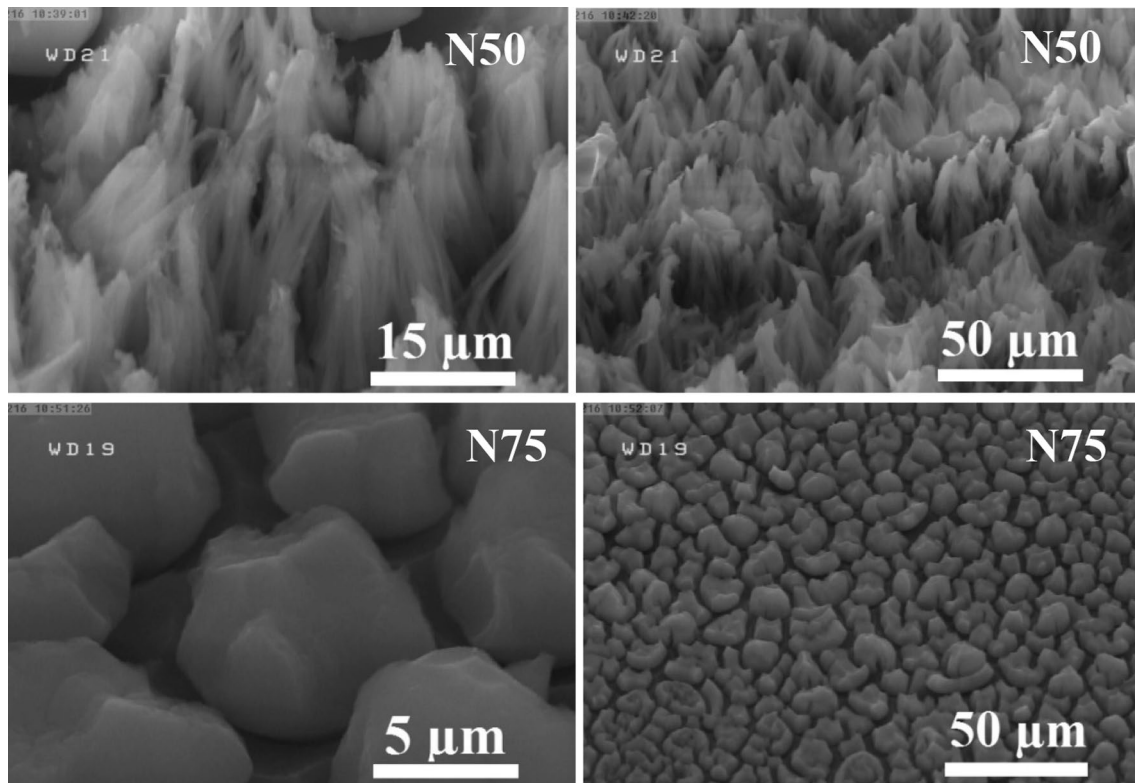


**Fig. 2** Oblique-view of FESEM images of N50 and N75 samples in various scales

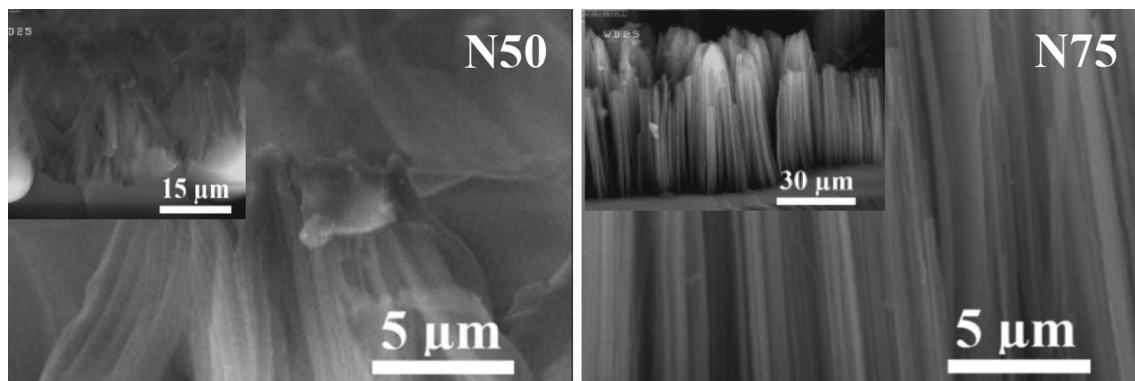


**Fig. 3** The FESEM cross-section images of N50 and N75 samples. The insets show the same view but with different scale

### 3.3 Vibrational properties

For further investigation of physical properties of the etched samples, Raman measurements were carried out with an excitation wavelength of 532 nm. Figure 6 presents the first order Raman spectra of bulk-Si and the SiNWs samples prepared at different etching temperatures. At first glance as it is clear after etching, Raman scattering intensity is dramatically increased compare to flat Si wafer. This behavior could be related to the reflectance data shown in Fig. 5. As it is expected a low percentage of reflectance could result to

increment of light intensity entering the samples and therefore, lead to a stronger Raman scattering intensity [21].

According to the published papers, the bulk-Si exhibits a Raman peak at  $519.8\text{ cm}^{-1}$ , which implies a first order optical phonon scattering [1, 21]. The transverse optical (TO) Raman mode is red-shifted for all SiNW samples ( $\omega_{N25} = 518\text{ cm}^{-1}$ ,  $\omega_{N50} = 517.1\text{ cm}^{-1}$ , and  $\omega_{N75} = 516.4\text{ cm}^{-1}$ ). The downshifts could be attributed to quantum confinement effect of optical phonons and/or to some extent the strain on the NWs and/or the formation of SiNCs within the NWs [22]. In our samples according to

**Fig. 4** TEM images and SAED patterns (the insets) of typical SiNWs in N50 and N75 samples

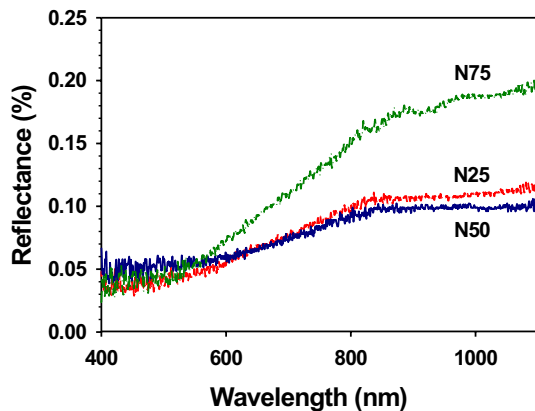
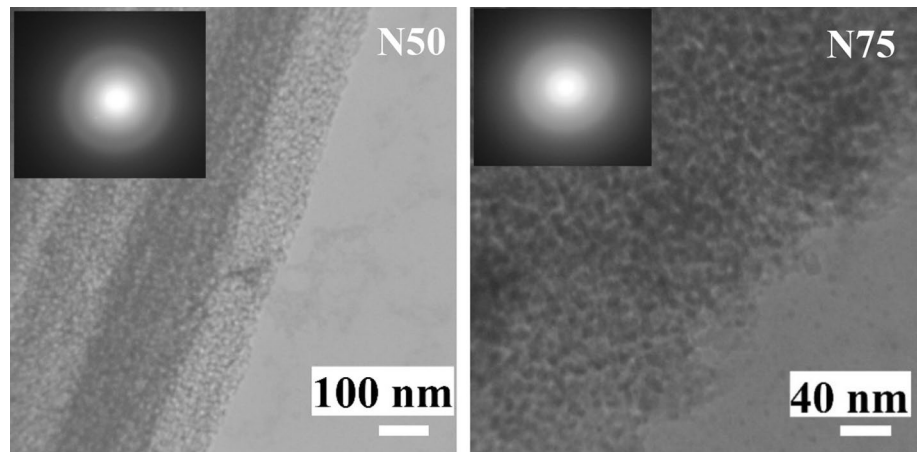


**Fig. 5** Reflectance spectra of the etched samples

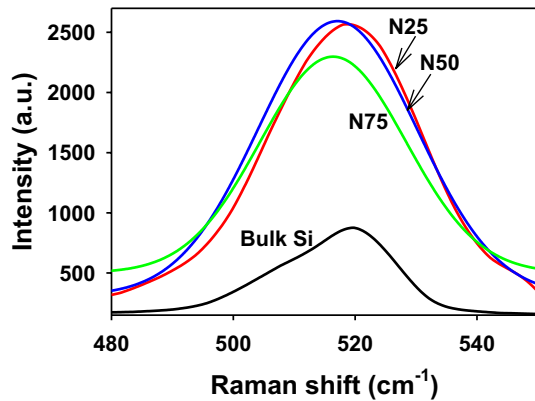


**Fig. 6** Raman spectra of bulk Si and as-prepared SiNWs

TEM images, which confirm that the surfaces of NWs are decorated with rough pores, we proceed with the possibility of formation of SiNCs as the main cause for the appearance of the relatively high Raman shifts ( $\sim 2\text{--}4\text{ cm}^{-1}$ ), also appearance and variations of the peak position of the studied samples' PL spectra (Sect. 3.4). According to the convenient

**Table 2** Detailed analysis of the studied samples based on Raman and also PL spectra data

Sample code	NW length ( $\mu\text{m}$ )	$\Delta\omega$ ( $\text{cm}^{-1}$ )	SiNC size (nm)	$\lambda_p$ (nm)	$E_p$ (eV)
N25	10	- 1.8	4.50	686	1.80
N50	25	- 3	3.51	684	1.81
N75	60	- 3.7	3.04	681	1.82

analytical model, we have tried to estimate the size of SiNCs from the Raman shifts data [1, 22, 23]:

$$\Delta\omega = -A\left(\frac{a}{L}\right)^\gamma \quad (5)$$

where the quantities  $\Delta\omega$ ,  $a$  ( $=0.543\text{ nm}$ ) and  $L$  are the Raman frequency shift, silicon lattice constant, and silicon crystallite size, respectively.  $A$  is a parameter equal to 52.3, and  $\gamma = 1.586$ . The evaluated nano-crystallite sizes are listed in Table 2. From this analysis, clearly with increasing the temperature of the etching solution the crystallite sizes are decreased from 4.50 nm in N25 to 3.04 nm in N75.

### 3.4 Photoluminescence (PL) properties

For further confirmation of presence SiNCs, Fig. 7 shows the visible PL spectra from as-prepared samples at different etching temperatures. According to these data the broadband PL peaks are centered ( $\lambda_p$ ) around 686, 684, and 681 nm, for N25, N50, and N75, respectively. Different mechanisms such as quantum confinement and  $\text{SiO}_x/\text{Si}$  interface defects and/or defect states on the surface of the oxide, related to the Si–O bond have been suggested to explain the PL emission from SiNWs [24, 25]. Since the diameter of SiNWs is very large compared to exciton Bohr radius in Si crystals (5 nm) [1], and indirect nature of the band gap of samples, the diameter size of the NWs may not be responsible for the visible PL. Considering Table 2, since the sizes of SiNCs are smaller

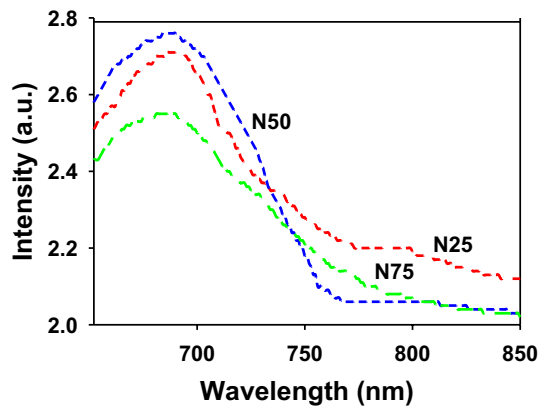


Fig. 7 PL spectra of as-prepared SiNWs

than the exciton Bohr radius together with the appearance of the broadband PL peaks, these evidences could be originated from SiNCs decorated on the NWs surfaces [18]. According to the creation and reduction in size of these nano crystallites on the wall of the NWs, and considering the occurrence of the quantum confinement effect, the PL peak position of the studied samples are decreased from 686 to 681 nm (corresponding to photon energies,  $E_p$ , of 1.80–1.82 eV) with increasing the solution temperature.

Also, as it is clear from PL data, the PL intensity is increased for N50 in comparison to N25, then decreased for N75. This could be explained according to the fact that a sample with higher surface porosity has a bigger surface to volume ratio, and therefore, light exposure area will increase. Hence more excited electrons will be created by the exciting laser beam. This explanation is in good agreement with the FESEM images of these samples (Fig. 2). According to these images in N75 due to the formation of longer NWs they are curved and formed bunches of wires which led to a low effective exposure surface, whereas in N50 the NWs are somehow vertically covered the wafer resulting in higher effective area.

## 4 Conclusions

We have successfully fabricated uniform arrays of mesoporous SiNWs through 1-MACE method at room temperature using lightly doped silicon wafer. The influence of etching solution temperature (RT, 50 and 75 °C) on physical properties of the prepared NWs has also been investigated. The FESEM and TEM images revealed that increasing the etching solution temperature from RT to 75 °C led not only to the increment of the length of NWs, gradually from 10 to 25 and 60  $\mu\text{m}$ , but also creation of dense mesoporous structures on the NWs. The SAED patterns of these wires indicated that although the SiNWs prepared at RT keep

their single-crystal structure, but those prepared at higher temperatures have a polycrystalline structure. According to the reflectance spectra in the range of 400–1100 nm, by comparing the bulk flat silicon wafer with the etched samples, we found out this quantity is strongly reduced ( $\sim 500$  times) as a result of mp-SiNWs formation. This extremely low reflectance can open up opportunities in photovoltaic applications. According to Raman peak shifts, mainly due to the formation of SiNCs on the sidewall of nanowires, we have estimated the decorated nano crystallite size on the surface of SiNWs that is decreased from 4.50 to 3.04 nm with increasing the solution temperature. The trend of these variations is consistent with peak positions of the visible PL spectra for these samples.

## References

1. M. Lajvardi, H. Eshghi, M. Ghazi, M. Izadifard, A. Goodarzi, *Mater. Sci. Semicond. Process.* **40**, 556–563 (2015)
2. A.I. Hochbaum, D. Gargas, Y.J. Hwang, P. Yang, *Nano Lett.* **9**(10), 3550–3554 (2009)
3. F. Bai, M. Li, D. Song, H. Yu, B. Jiang, Y. Li, *J. Solid State Chem.* **196**, 596–600 (2012)
4. F. Patolsky, B.P. Timko, G. Yu, Y. Fang, A.B. Greytak, G. Zheng, C.M. Lieber, *Science.* **313**(5790), 1100–1104 (2006)
5. W.-K. To, C.-H. Tsang, H.-H. Li, Z. Huang, *Nano Lett.* **11**(12), 5252–5258 (2011)
6. Y. Qu, L. Liao, Y. Li, H. Zhang, Y. Huang, X. Duan, *Nano Lett.* **9**(12), 4539–4543 (2009)
7. Y. Qu, H. Zhou, X. Duan, *Nanoscale.* **3**(10), 4060–4068 (2011)
8. D. Kumar, S.K. Srivastava, P. Singh, K. Sood, V. Singh, N. Dilawar, M. Husain, *J. Nanopart. Res.* **12**(6), 2267–2276 (2010)
9. Z. Huang, J. Liu, *JSM Nanotechnol Nanomed.* **3**(1), 1035–1031 (2015)
10. B. Miao, J. Zhang, X. Ding, D. Wu, Y. Wu, W. Lu, J. Li, *J. Micro-mech. Microeng.* **27**(5), 055019 (2017)
11. Z. Huang, N. Geyer, P. Werner, J. De Boor, U. Gösele, *Adv. Mater.* **23**(2), 285–308 (2011)
12. S. Niazorau, K. Girel, A. Sherstnyov, E. Chubenko, H. Bandarenka, V. Bondarenko, *Phys. Status solidi.* **13**(4), 146–150 (2016)
13. W.M. Shaoyuan, Li, Y. Zhou, X. Chen, Y. Xiao, M. Ma, W. Zhu, F. Wei, *Nanoscale Res. Lett.* **9** (2014)
14. C. Chiappini, X. Liu, J.R. Fakhoury, M. Ferrari, *Adv. Funct. Mater.* **20**(14), 2231–2239 (2010)
15. G. Oskam, J. Long, A. Natarajan, P. Searson, *J. Phys. D.* **31**(16), 1998 (1927)
16. H. Chen, R. Zou, H. Chen, N. Wang, Y. Sun, Q. Tian, J. Wu, Z. Chen, J. Hu, *J. Mater. Chem.* **21**(3), 801–805 (2011)
17. C.Y. Chen, C.S. Wu, C.J. Chou, T.J. Yen, *Adv. Mater.* **20**(20), 3811–3815 (2008)
18. R. Ghosh, P. Giri, K. Imakita, M. Fujii, *Nanotechnology.* **25**(4), 045703 (2014)
19. K. Peng, J. Hu, Y. Yan, Y. Wu, H. Fang, Y. Xu, S. Lee, J. Zhu, *Adv. Funct. Mater.* **16**(3), 387–394 (2006)
20. M.-L. Zhang, K.-Q. Peng, X. Fan, J.-S. Jie, R.-Q. Zhang, S.-T. Lee, N.-B. Wong, *J. Sci.* **4**(8), 2863–2869 (2011)
21. H.-C. Chang, K.-Y. Lai, Y.-A. Dai, H.-H. Wang, C.-A. Lin, J.-H. He, *Energy Environ. Sci.* **4**(8), 2863–2869 (2011)

22. S. Piscanec, M. Cantoro, A. Ferrari, J. Zapien, Y. Lifshitz, S. Lee, S. Hofmann, J. Robertson, *Phys. Rev. B.* **68**(24), 241312 (2003)
23. C.M. Hessel, J. Wei, D. Reid, H. Fujii, M.C. Downer, B.A. Korgel, *J. Phys. Chem. Lett.* **3**(9), 1089–1093 (2012)
24. A. Najar, A. Slimane, M.N. Hedhili, D. Anjum, R. Sougrat, T. Ng, B. Ooi, *J. Appl. Phys.* **112**(3), 033502 (2012)
25. V.A. Sivakov, F. Voigt, A. Berger, G. Bauer, S.H. Christiansen, *Phys. Rev. B.* **82**(12), 125446 (2010)